euspen's 21st International Conference & Exhibition, Copenhagen, DK, June 2021

www.euspen.eu

Closed-loop force control methods for linear flexible stages using voice-coil linear actuator

Daniel Grivon[1], Lionel Bischof[1], Yves-Julien Regamey[1], Emmanuel Onillon[1], Hervé Saudan[1], Leopoldo Rossini[1]

[1]*Swiss Center for Electronics and Microtechnology (CSEM SA), CH-2002, Neuchâtel, Switzerland*

leopoldo.rossini@csem.ch, daniel.grivon@csem.ch

Abstract

The proposed extended abstract describes strategies to control the contact force between a moving end effector and a highly dynamic environment with only partially known characteristics. The control strategies will be applied to two distinct applications in the field of biological sensing and machine tools, which are characterised by different force amplitudes (i.e. from mN to kN), control accuracy, and dynamic environment. For both strategies, the force is impaired through a linear voice-coil actuator with moving part guided with flexible blades that is operated in closed-loop force control fashion. Two distinct approaches for closed-loop control synthesis will be presented. The first method relies on classical LQR state-feedback with a force estimator. The second method is based on a frequency-domain design through the definition of H_∞ performance constraints of the closed-loop sensitivity function. Additionally, a practical bumpless position-to-force control switching will be presented.

Force, Feedback control, Flexible blade, Mechatronics, Actuator, Voice-coil, H_∞.

1. Introduction

Research on closed-loop force control has prospered in the past decades with multiple successful applications especially in the field of robotics, where the purpose is to control the interaction of an end effector with the environment. Relevant examples include telemedicine, haptics feedback, robot manipulation, with several practical tasks include polishing, deburring, machining, or assembly. Nevertheless, pure position control is predominant and systems aiming to control force and position, as well as their switching, are less common. In the presented work, two distinct approaches for closed-loop control synthesis will be introduced for two different systems which are characterised by different force amplitudes (i.e. from mN to kN), control accuracy, and dynamic environment. Bumpless controller switching is usually implemented to avoid bumps for the open to closed loop transition and are usually related to PID controllers [1], while implementation for higher order controllers are missing. Firstly a description of the systems is given in section 2. To underline the similar architecture despite the difference in scale and output force ranges, an only block diagram will be used to describe both the systems. Successively, sections 3 and 4 describe the control strategies implemented on each systems as well as the main results achieved. Section 5 presents the implementation details allowing to achieve the bumpless force-to-position (and viceversa) controller switching for PID like controllers and for higher order (> 5) controllers.

2. Systems description

Both the systems are based on a similar architecture in which the force or position of the end effector is controlled using a Voice Coil Actuator (VCA) which is guided using a simple parallelogram flexure mechanism (Figure 1). Nevertheless, the scale of the two systems is largely different (Table 1).

Table 1: Main parameters of systems under study.

	SYSTEM #1	SYSTEM #2	
m_1	0.011	120	(kg)
m_2	N.A.	15	(kg)
m_3	≈ 0.1	2	(kg)
K_{flex}	0.556	140	(N/mm)
K_{VCA}	4.42	124.7	(N/A)
Continuous VCA Force	1	500	(N)
Peak VCA Force	1	1860	(N)

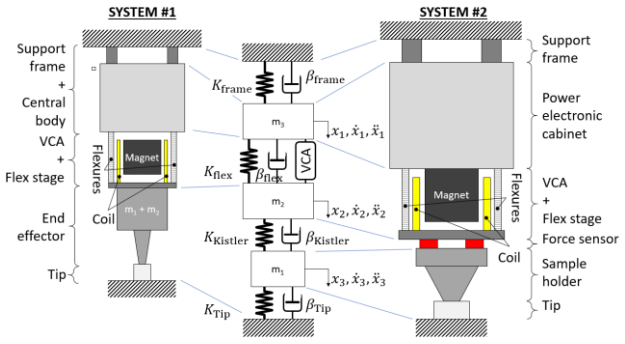

Figure 1. Mass-damper-spring-model to represent the both systems (pictures of real systems unavailable due to confidentiality agreement).

No force sensor is present in system #1, thus masses m_1 and m_2 appears as single m_1 mass. The VCA is a custom built unit by CSEM, its position measurement relies on a miniature inductive encoder from POSIC. The electronics used for testing is a dSPACE microlabbox and a custom built power amplifier.

System #2 is an appendix of a more complex tooling workstation. The VCA is a BEI-Kimco LA50-65-000 driven by a LCAM-5/15 Linear Amplifier from H2W. A force sensor used is a Kistler 9046C4 dynamometer kit including 4 triaxial ring force transducers. An Eddy's current sensor EddyNCDT3010 from Micro-Epsilon is used for VCA position measurement.

3. System #1: Force control using force estimator

The apparatus described under system #1 is used to apply precise and small forces. The small size, low forces and price constraints on the final application prevented the use of a force sensor. The system has two operating modes and force application. Hereunder a typical operational sequence:

1) Approach: non contact and position control
2) Contact: estimation of external forces to reach a threshold
3) Braking to zero speed
4) Applying a force trajectory.

In order to achieve this behaviour the system needs:

- Position controller
- A force estimator
- A force controller

Positon control is based on a LQR regulator [3] with the following system states, position, speed (estimated), current, integral of position error. A non linear feedforward is added to improve the braking time and to limit the force overshoot just after contact. Contact is defined with a threshold on the external force, the latter being estimated as the difference between the VCA force and the spring force from the flexure blade (F_{ks}), optionally a term accounting for inertial forces can be added. The strategy used to control the force is based on computing the required current to apply the desired forces. The required current is:

$$i_{ref}(x, F_{ref}) = \frac{F_{ref} + F_{ks}(x)}{K_m(x)}$$

A digital loop is used to compute the required voltage to obtain the said current.

$$U = (K_p + \frac{K_i}{z-1}) \cdot (i - i_{ref})$$

Where Ki, Kp are calculated to achieve a 200 Hz bandwidth. Note that the sampling time of the current loop is set to 5 kHz. The openloop bode plot of the full system in contact with a surface is depicted in Figure 2. Contact surface is particularly soft with stiffnesses ranging from 30 N/m up to 600 N/m. The current bandwith is set to 200 Hz but the complete system bandwidth is lower due to the surface interactions (see Figure 3). The main challenge in this application is the calibration of F_{ks} and $K_m(x)$ motor constant versus position. Moreover to have accurate force, the flexure stage has to be free from bi-stable behaviour and hysteresis.

3.1. Results

The system developed is able to maintain a force on a soft surface with an accuracy of about ± 5mN, without any force sensor.

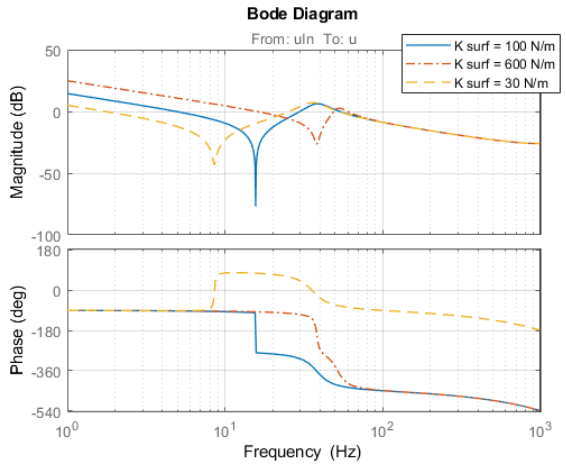

Figure 2. Open loop of current controller, system and surface interaction, for diverse surfaces stiffnesses.

Closing the loop lead to the step responses depicted in Figure 3.

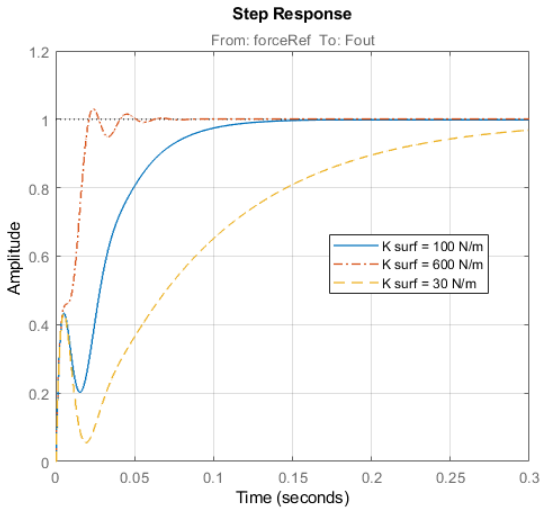

Figure 3. Step response of current controller, system and surface interaction, for diverse surfaces stiffnesses.

4. System #2: Force control using H_∞

As already introduced, system #2 can be seen as a sub-system embedded in a more complex machine composed of different sub-systems. This means that the operations performed by the other machine subsystems are seen by system #2 as induced perturbations on the quantity to be controlled, i.e. on the tool tip. Consequently, the two main functions 2dentify2hed

1. **Position control**: put in contact (or detach) the system end-effector to the part to be machined
2. **Force control**: ensure the reference force traking as well as the rejection of the induced perturbations during the most critical operating phases.

The machine process is such that the mechanical properties of end-effector varies during operation. In such case, applying classical model-based system description for controller synthesis covering the whole operating scenario is rather difficult. Moreover, closed-loop system identification is required to define system variations during operation. Consequently, data-driven controller synthesis method is more suitable [4]. In particular, an H_∞ design approach is used. Initially a controller is designed using Open-Loop (OL) identification data. Successively Closed Loop (CL) identification data are used for controller design refinement for optimal perturbation rejection.

4.1. Open loop identification and initial controller design

External perturbations can be either induced by other machine subsystems either unmodelled dynamics.

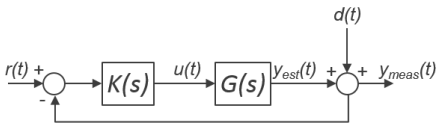

Figure 4. Basic feedback control scheme.

The perturbations $d(t)$ acting on the output can be defined as

$$d(t) = y_{meas}(t) - y_{est(t)} = y_{meas}(t) - \hat{G}(s) \cdot u(t)$$

Where $u(t)$ is the VCA current and $y_{meas}(t)$ is the contact force and $\hat{G}(s)$ is the plant model identified in OL (Figure 5).

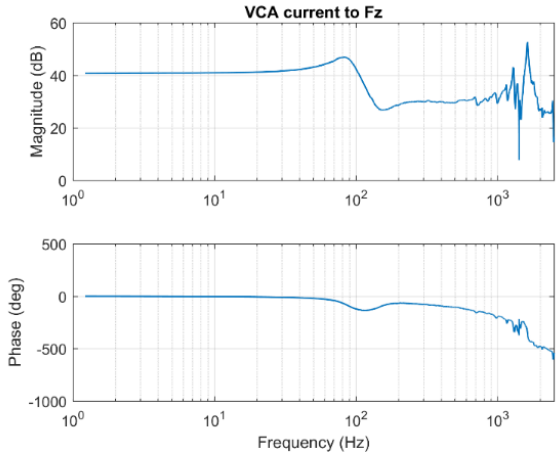

Figure 5. Transfer fuction from VCA current to $\boldsymbol{F_z}$.

The controller $K(s)$ is designed using the Frequency-Domain Robust Control (FDRC) Toolbox from EPFL [4] so that the sensitivity function $S(s)$ satisfies the following H_∞ criterion

$$\|W_1(j\omega)S(j\omega)\|_\infty < 1 \leftrightarrow |S(j\omega)| < |W_1(j\omega)|^{-1}, \forall\omega \quad (2)$$

The weighting function $W_1^{-1}(s)$ is designed as a mask to attenuate eventual perturbations in the frequency range below 100 Hz by 13dB, while allowing $S(s)$ to rise to values up to 6 dB starting from the frequency of 100 Hz.

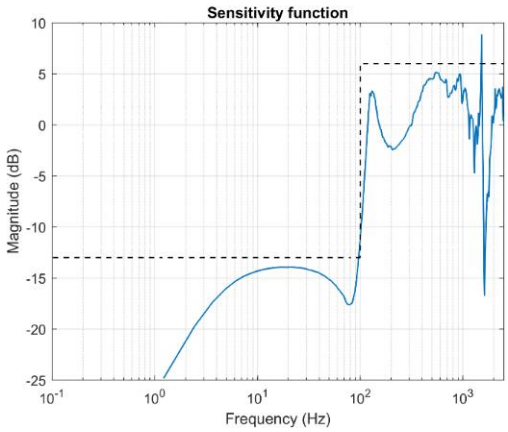

Figure 6. The weighting function $\boldsymbol{W_1^{-1}(s)}$ (dashed line) and the $\boldsymbol{S(s)}$ obtained with the initially designed controller.

The main constraints for the controller design are the presence of an integrator and the controller order, which is limited to 5.

4.2. Closed Loop Identification and Iterative Controller Design

CL identification based on spectral analysis is performed when normal machine operation regime is achieved, i.e. when steady state is achieved. If the length of each pass is too short and it prevent the gathering of enough data to correctly 3dentify the system, a transfer function is determined for each pass., the identified transfer functions are averaged with the aim to reduce the variability due to noise measurements. Figure 7 depicts the transfer functions identified for the same load but for different operating conditions of the external sub-system (for example different machining speeds). The speed dependence is clearly visible, causing a shift of the characteristic, at least for what concerns frequency range [10-110] Hz, to the left.

The first step for the controller synthesis is to define the perturbations $d(t)$ on the output for each newly determined $\hat{G}(s)$. After having defined the main frequency content of the force $F_z(t)$ obtained with the initial controller, new constraints on the sensitivity function can be defined to reduce their influence on some specific frequency range.

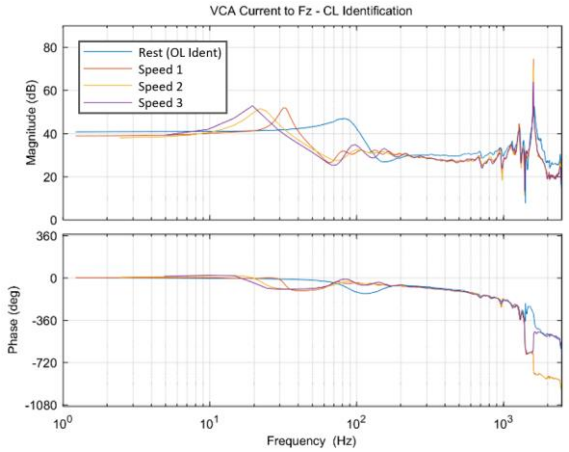

Figure 7. Transfer function identified in CL for a load for a same load.

4.3. Results

After having observed the frequency distribution of the force with the initial controller, the $W_1^{-1}(s)$ displayed in Figure 8b (dashed line) has been designed to attenuate the interested frequencies, below 100 Hz and above 1 kHz. The constraint on the controller order is relaxed and a controller with order 20 has been found to satisfy the H_∞ criterion for this particular case.

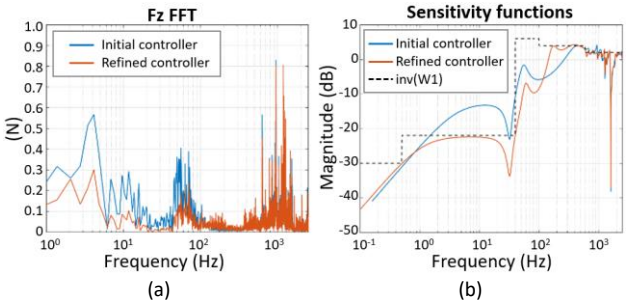

Figure 8. (a) Comparison of the F_z spectra obtained with the initial controller and the refined controller. (b) Comparison of the sensitivity functions of the two controllers.

5. Bumpless position-to-force control switching

Both mechanical systems has to switch between OL, position and force control. Two possible solutions to implement bumpless controller switching are presented here, one for each system. In both cases the requirement essentially comes down to initalising the controller "memory" correctly so the outputs of the 2 controllers at switching time t^* match.

A. System 1:

For the first system a switch between a PI force controller and an LQR position controller is required: the integrator of the inactive controller is initalised by reverse computation. The force PI controller is written as

$$u(t) = K_P e(t) + K_i \frac{T_s}{z-1} e(t)$$

Where u is the controller output, e its input (error), T_s the sampling time and K_P, K_i the PI gains. When switching from position (or open loop) to force, the I term is initialized to the current measured output $u(t)$ minus the proportional term

$$I_0 = u_{meas}(t) - K_P e(t) \rightarrow u(t) = K_P e(t) + I_0 = u_{meas}(t).$$

For position control, an LQR is used with the estimated states being the position, speed and current of the actuator

$$u(t) = K_i \frac{T_s}{z-1} e(t) - [K_1 \quad K_2 \quad K_3] \begin{bmatrix} p(t) \\ v(t) \\ i(t) \end{bmatrix}$$

Where K_1, K_2, K_3 are the LQR gains and p, v, i are the position, speed and current making out the system state vector. Similarly, when switching to position control, the integrator is initialized to the current output minus the LQR term.

$$I_0 = u_{meas}(t) + [K_1 \quad K_2 \quad K_3]\begin{bmatrix} p(t) \\ v(t) \\ i(t) \end{bmatrix}$$

This scheme has the advantage of working independent of the system being in steady-state.

B. System 2:

For the second system switching is between a PID position controller and a H_∞ force controller. Both controllers are implemented with a difference equation intrinsically providing bumpless switching if the correct controller inputs are used.

Given $u(t) = \frac{b_0 + b_1 q^{-1} + b_2 q^{-2} + \cdots + b_{n_B} q^{-n_B}}{1 + a_1 q^{-1} + a_2 q^{-2} + \cdots + a_{n_A} q^{-n_A}} e(t)$ where u is the controller output, e its input (error) and b_n, a_n its numerator and denominator coefficients respectively, which is

$$A(q^{-1})u(t) = B(q^1)e(t).$$

If we pose

$$\underline{\text{Position}}: \quad A_P(q^{-1})u_P(t) = B_P(q^1)[r_p(t) - y_P(t)]$$
$$\underline{\text{Force}}: \quad A_F(q^{-1})u_F(t) = B_F(q^1)[r_F(t) - y_F(t)]$$

then when one controller is in use, the reference is replaced by the current measurement, i.e. $r(t) = y(t)$, and the computed force controller outputs by the measured position controller outputs, i.e. $u_F(t-n) = u_P(t-n)$. Thus, when in position control and steady-state, we get

$$r_P(t) = y_P(t) \rightarrow A_P(q^{-1})u_P(t) = 0$$

Due to the integrator and steady-state, we know that

$$\sum_{i=0}^{n_{Ap}} a_{ip} = 0 \quad \text{and} \quad 1 = -a_{1p} - a_{2p} - \cdots - a_{n_{Ap}}$$

And similarly for the force controller

$$A_F(q^{-1})u_F(t) = 0$$
$$1 = -a_{1F} - a_{2F} - \cdots - a_{n_{AF}}$$
$$u_F(t) = \left[-a_{1F}q^{-1} - a_{2F}q^{-2} - \cdots - a_{n_{AF}}q^{-n_{AF}}\right]u_F(t)$$

Replacing past $u_F(t)$ by past $u_P(t)$ it follows that

$$u_F(t) = u_P(t)$$

So, both controller ouputs at time t^*, in steady-state, are equal.

5.1. Results

Figures 9 to 11 provides evidences of the quality of the bumpless position → force → position transition achieved.

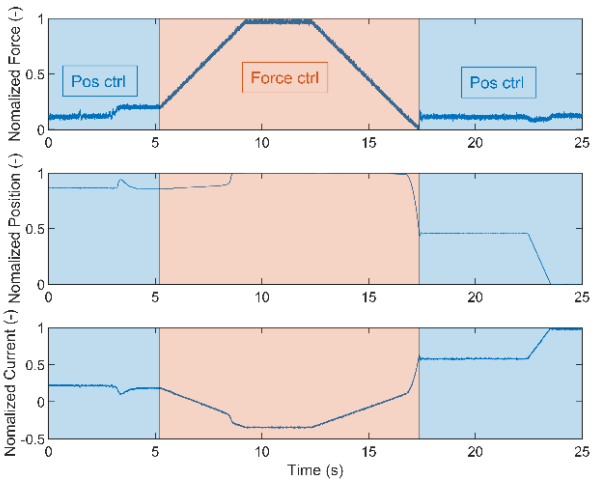

Figure 9. System 1 controller transitions.

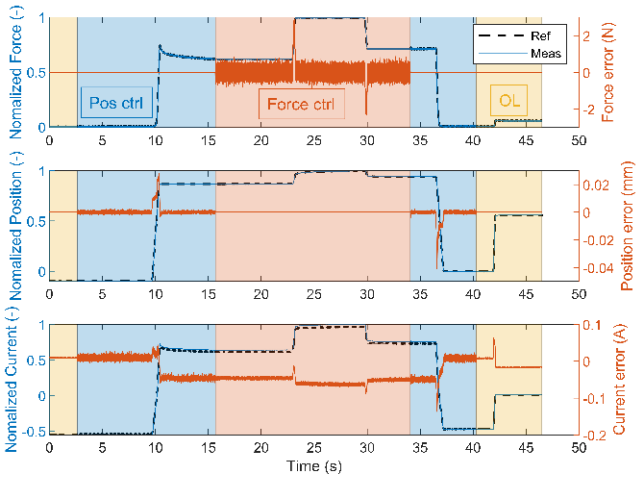

Figure 10. System 2 controller transitions.

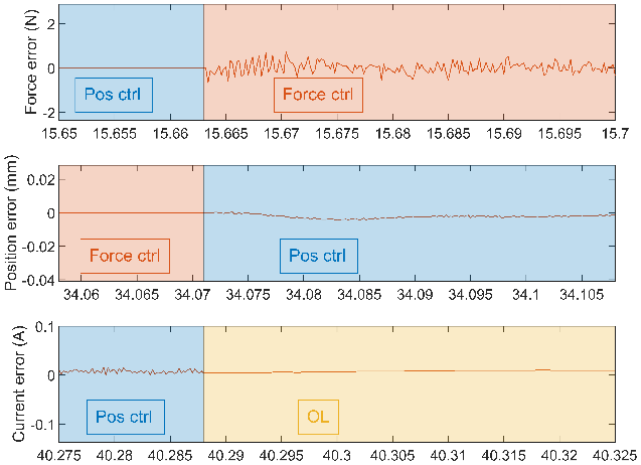

Figure 11. System 2 zoom on switching zones.

6. Conclusions

In the presented work two different approaches for force controller synthesis have been discussed, in relation to two different mechanical systems, both of them based on the moving stage architecture VCA+Flexure. The preferred solutions implemented to overcome the two main challenges, i.e. force estimation for System #1 and perturbation rejection for System #2, have been detailly presented with results assessing the validity of the approaches. Last, but not least, two methods to achieve bumpless switching from position to force control and vice-versa have been presented for classical LQR controller and less common high order H_∞ controllers, one for each system, and demonstrated to be effective.

References

[1] - G. F. Franklin, D. J. Powell, M. L. Workman, Digital Control of Dynamic Systems, Addison-Wesley, 1998.

[2] - K. Åström, T. Hägglund, Advanced PID Control, ISA, Research Triangle Park, NC, August 2005.

[3] - I. Landau, R. Lozano, M. M'Saad, A. Karimi, Adaptive Control: Algorithms, Analysis and Applications, Springer, 2nd Edition, 2011.

[4] - Frequency Domain Robust Control (FDRC) Toolbox, https://www.epfl.ch/labs/la/research/page- 67797-en-html/page-67814-en-html/fdrc_toolbox/ .